

A hybrid seesaw model and hierarchical neutrino flavor structures based on A_4 symmetry

Mayumi Aoki^{1,*} and Daiki Kaneko^{1,†}

¹*Institute for Theoretical Physics, Kanazawa University, Kanazawa 920-1192, Japan*

Abstract

We propose a hybrid seesaw model based on A_4 flavor symmetry, which generates a large hierarchical flavor structure. In our model, tree-level and one-loop seesaw mechanisms predict different flavor structures in the neutrino mass matrix and generate a notable hierarchy among them. We find that such a hierarchical structure gives a large effective neutrino mass that can be accessible by next-generation neutrinoless double beta decay experiments. Majorana phases can also be predictable. The A_4 flavor symmetry in the model is spontaneously broken to the Z_2 symmetry, leading to a dark matter candidate that is assumed to be a neutral scalar field. The favored mass region of the dark matter is obtained by numerical computations of the relic abundance and the cross section of the nucleon. We also investigate the predictions of several hierarchical flavor structures based on A_4 symmetry for the effective neutrino mass and the Majorana phases, and find characteristic features depending on the hierarchical structures.

arXiv:2009.06025v2 [hep-ph] 8 Mar 2021

* mayumi@hep.s.kanazawa-u.ac.jp

† d_kaneko@hep.s.kanazawa-u.ac.jp

I. INTRODUCTION

The discovery of neutrino oscillations shows that neutrinos are mixed with each other and have tiny masses. Since neutrinos are massless particles in the Standard Model (SM), new physics beyond the SM that has some mechanism to generate the neutrino masses is required. The Type-I seesaw mechanism [1–5] is one of the attractive ways to generate such tiny neutrino masses at tree level, which requires an introduction of right-handed neutrinos. Another attractive way to explain the tiny masses is a radiative seesaw mechanism in which neutrino masses are generated by loop effects (see Refs. [6–12] for early works and also Ref. [13] for a later review). In radiative seesaw models involving right-handed neutrinos [9–11] a discrete symmetry is imposed to forbid the Type-I seesaw mechanism. This symmetry is also responsible for the stability of dark matter (DM).

The neutrino mass matrix is diagonalized by the lepton flavor mixing matrix, the so-called Pontecorvo-Maki-Nakagawa-Sakata (PMNS) matrix, which is parameterized as

$$U_{\text{PMNS}} = \begin{pmatrix} c_{12}c_{13} & s_{12}c_{13} & s_{13}e^{-i\delta} \\ -s_{12}c_{23} - c_{12}s_{23}s_{13}e^{i\delta} & c_{12}c_{23} - s_{12}s_{23}s_{13}e^{i\delta} & s_{23}c_{13} \\ s_{12}s_{23} - c_{12}c_{23}s_{13}e^{i\delta} & -c_{12}s_{23} - s_{12}c_{23}s_{13}e^{i\delta} & c_{23}c_{13} \end{pmatrix} \begin{pmatrix} 1 & 0 & 0 \\ 0 & e^{i\alpha_2/2} & 0 \\ 0 & 0 & e^{i\alpha_3/2} \end{pmatrix}, \quad (1)$$

where $c_{ij} = \cos \theta_{ij}$ and $s_{ij} = \sin \theta_{ij}$ for $i, j = 1, 2, 3$. The parameter δ is a Dirac phase, while α_2 and α_3 denote Majorana phases. The data obtained in neutrino oscillation experiments [14–18] show that the neutrino mixing angles are $\theta_{12} \simeq 33^\circ$, $\theta_{23} \simeq 49^\circ$, $\theta_{13} \simeq 8.6^\circ$, and the neutrino mass-squared differences $\Delta m_{31}^2 \equiv m_3^2 - m_1^2$ and $\Delta m_{21}^2 \equiv m_2^2 - m_1^2$ are $|\Delta m_{31}^2| \simeq 2.5 \times 10^{-3} \text{ eV}^2$ and $\Delta m_{21}^2 \simeq 7.4 \times 10^{-5} \text{ eV}^2$, respectively. The recent measurements of the Dirac phase show $\delta = 107^\circ \rightarrow 403^\circ$ for the normal mass ordering (NO) and $\delta = 192^\circ \rightarrow 360^\circ$ for the inverted mass ordering (IO) at 3σ CL [19]. The mixing matrix has two large mixings, which is very different from the quark mixing. Apart from the tiny masses of neutrinos, such flavor structures will give us hints of physics beyond the SM.

One candidate behind the lepton sector is non-Abelian discrete flavor symmetries, such as S_3 , A_4 and S_4 (see Refs. [20–25] for reviews).¹ In particular, the study of the A_4 models has received considerable interest. It has been shown in Ref. [27] that the A_4 flavor symmetry leads naturally to the neutrino mass matrix that gives tri-bimaximal flavor mixing, M_{Tri} (*i.e.*, $s_{12} = 1/\sqrt{3}$, $s_{23} = 1/\sqrt{2}$, $s_{13} = 0$) [28]. It is known that M_{Tri} is given by a linear combination of three flavor structures as

$$M_{\text{Tri}} = \frac{m_1 + m_3}{2} \begin{pmatrix} 1 & 0 & 0 \\ 0 & 1 & 0 \\ 0 & 0 & 1 \end{pmatrix} + \frac{m_2 - m_1}{3} \begin{pmatrix} 1 & 1 & 1 \\ 1 & 1 & 1 \\ 1 & 1 & 1 \end{pmatrix} + \frac{m_1 - m_3}{2} \begin{pmatrix} 1 & 0 & 0 \\ 0 & 0 & 1 \\ 0 & 1 & 0 \end{pmatrix}. \quad (2)$$

¹ Applications of modular symmetries to explain the neutrino flavor structure have been proposed (see *e.g.*, Ref.[26]), where the Yukawa couplings are restricted by the modular symmetry.

However, since the observed value of θ_{13} is small but non-zero, the neutrino mass matrix should be modified from M_{Tri} so as to realize the non-zero (1,3) off-diagonal element in the flavor mixing matrix. One possible form of the neutrino mass matrix that derives the non-zero θ_{13} is given by adding another new flavor structure as [29]

$$M_\nu = a \begin{pmatrix} 1 & 0 & 0 \\ 0 & 1 & 0 \\ 0 & 0 & 1 \end{pmatrix} + b \begin{pmatrix} 1 & 1 & 1 \\ 1 & 1 & 1 \\ 1 & 1 & 1 \end{pmatrix} + c \begin{pmatrix} 1 & 0 & 0 \\ 0 & 0 & 1 \\ 0 & 1 & 0 \end{pmatrix} + d \begin{pmatrix} 0 & 0 & 1 \\ 0 & 1 & 0 \\ 1 & 0 & 0 \end{pmatrix}, \quad (3)$$

where the coefficients of each flavor structure a , b , c and d are the arbitrary-mass dimensional parameters. The non-vanishing d term in the models with A_4 symmetry is discussed in Refs. [21, 29–34]. It is expected that the relationship between these four flavor structures will provide us with important information on the flavor symmetry in the neutrino mass generation mechanism.

In this paper, we propose a hybrid seesaw model based on the non-Abelian A_4 flavor symmetry, in which the neutrino mass matrix Eq. (3) is generated by the tree-level and the one-loop seesaw mechanisms.² These mechanisms generate different flavor structures, which leads to a characteristic hierarchy between the coefficients of the four flavor structures. The d term in Eq. (3) comes from the one-loop seesaw mechanism. Two benchmark points are chosen in our model and their predictions for the effective neutrino mass and the Majorana CP phases are computed. Before presenting the results in our model, we also show the predictions of a model-independent analysis by using Eq. (3) for some cases with hierarchical flavor structure. The A_4 symmetry in our model is broken into the Z_2 subgroup by the vacuum expectation value (VEV) of the A_4 triplet scalar field. Therefore, the lightest neutral Z_2 -odd field, where we assume it to be a CP-even neutral scalar field, is stable and becomes a DM candidate. We compute the relic abundance and the spin-independent cross section of the DM, and show the plausible mass region of the DM.

II. MODEL

The non-Abelian A_4 flavor symmetry has four irreducible representations which are three singlets $\mathbf{1}$, $\mathbf{1}'$ and $\mathbf{1}''$ and one triplet $\mathbf{3}$. The A_4 symmetry is generated by two elements S and T ,

$$S = \begin{pmatrix} 1 & 0 & 0 \\ 0 & -1 & 0 \\ 0 & 0 & -1 \end{pmatrix}, \quad T = \begin{pmatrix} 0 & 1 & 0 \\ 0 & 0 & 1 \\ 1 & 0 & 0 \end{pmatrix},$$

² Other hybrid seesaw models based on the A_4 flavor symmetry have been considered in Refs. [30, 35–46].

	A_4	$SU(2)$	Z_2
(L_e, L_μ, L_τ)	$1, 1'', 1'$	2	$(+, +, +)$
$(l_{e_R}, l_{\mu_R}, l_{\tau_R})$	$1, 1', 1''$	1	$(+, +, +)$
(N_1, N_2, N_3)	3	1	$(+, -, -)$
H	1	2	+
$\eta = (\eta_1, \eta_2, \eta_3)$	3	2	$(+, -, -)$

TABLE I. A_4 flavor and $SU(2)$ gauge quantum numbers for leptons, right-handed neutrinos and scalar fields of the model.

which fulfill the relations $S^2 = T^3 = (ST)^3 = I$. The A_4 triplets $3_a = (a_1, a_2, a_3)$ and $3_b = (b_1, b_2, b_3)$ have the following multiplication rules:

$$\begin{aligned}
[3_a \otimes 3_b]_1 &= a_1 b_1 + a_2 b_2 + a_3 b_3, \\
[3_a \otimes 3_b]_{1'} &= a_1 b_1 + \omega a_2 b_2 + \omega^2 a_3 b_3, \\
[3_a \otimes 3_b]_{1''} &= a_1 b_1 + \omega^2 a_2 b_2 + \omega a_3 b_3, \\
[3_a \otimes 3_b]_{3_1} &= (a_2 b_3, a_3 b_1, a_1 b_2), \\
[3_a \otimes 3_b]_{3_2} &= (a_3 b_2, a_1 b_3, a_2 b_1),
\end{aligned}$$

where $\omega = e^{\frac{2\pi}{3}i}$ which satisfies $1 + \omega + \omega^2 = 0$.

We introduce three A_4 triplet right-handed neutrinos N_i ($i = 1, 2, 3$), which are invariant under the SM gauge group, and three A_4 triplet $SU(2)$ scalar doublets η_i . Model assignments are shown in Table I, where the A_4 singlets L_e, L_μ, L_τ ($l_{e_R}, l_{\mu_R}, l_{\tau_R}$) are lepton doublets (lepton singlets) and the A_4 singlet H is a Higgs doublet field. In this model, the Yukawa sectors of neutrinos are described by

$$\begin{aligned}
\mathcal{L}_{\text{Yukawa}} &= y_1 \overline{L_e} (\tilde{\eta}_1 N_1 + \tilde{\eta}_2 N_2 + \tilde{\eta}_3 N_3) + y_{1'} \overline{L_\mu} (\tilde{\eta}_1 N_1 + \omega \tilde{\eta}_2 N_2 + \omega^2 \tilde{\eta}_3 N_3) \\
&\quad + y_{1''} \overline{L_\tau} (\tilde{\eta}_1 N_1 + \omega^2 \tilde{\eta}_2 N_2 + \omega \tilde{\eta}_3 N_3) + \text{h.c.},
\end{aligned} \tag{4}$$

where $y_1, y_{1'}$ and $y_{1''}$ are the Yukawa couplings and $\tilde{\eta}_i = i\sigma^2 \eta_i^*$. In this work we assume $y \equiv y_1 = y_{1'} = y_{1''}$ for simplicity,³ where y is real. Majorana mass terms of right-handed neutrinos are given by

$$\begin{aligned}
\mathcal{L}_{\text{Majorana}} &= M_R (\overline{N_1^c} N_1 + \overline{N_2^c} N_2 + \overline{N_3^c} N_3) + M'_R (\overline{N_1^c} N_1 + \omega \overline{N_2^c} N_2 + \omega^2 \overline{N_3^c} N_3) \\
&\quad + M''_R (\overline{N_1^c} N_1 + \omega^2 \overline{N_2^c} N_2 + \omega \overline{N_3^c} N_3) + M_{23} (\overline{N_2^c} N_3 + \text{h.c.}),
\end{aligned} \tag{5}$$

where M_R, M'_R, M''_R and M_{23} are the Majorana masses of right-handed neutrinos. We note that the second, third, and fourth terms in Eq. (5) break the A_4 symmetry.⁴ Because of the fourth

³ The exact alignment of the Yukawa coupling ($y_1 = y_{1'} = y_{1''}$) is not necessary to explain the oscillation parameters. The deviations of $y_{1'}$ and $y_{1''}$ from y_1 are respectively within about 7 % and 3 % for explaining the observed neutrino oscillation parameters at 3σ CL [19].

⁴ These three terms can be generated by A_4 singlet $1'', 1'$ and triplet 3 scalar fields, respectively (the generation of the fourth term is discussed in, *e.g.*, Ref. [47]).

term, the neutrinos N_2 and N_3 are mixed with each other. The mass matrix of right-handed neutrinos is diagonalized by the complex mixing angle $\tan 2\hat{\theta}_R \equiv \frac{2M_{23}}{(\omega - \omega^2)(M_R'' - M_R')}$, where we define the diagonal elements as $(M_1, M_2 e^{i\delta_{R2}}, M_3 e^{i\delta_{R3}})$. Throughout this paper, we work in the basis where the charged lepton mass matrix is diagonal.

Based on the A_4 symmetry, the scalar potential is given by [48]

$$\begin{aligned}
V = & \mu_\eta^2 [\eta^\dagger \eta]_1 + \mu_H^2 H^\dagger H + \lambda_1 (H^\dagger H)^2 + \lambda_2 [\eta^\dagger \eta]_1^2 + \lambda_3 [\eta^\dagger \eta]_{1'} [\eta^\dagger \eta]_{1''} \\
& + \lambda_4 [\eta^\dagger \eta]_{1'} [\eta \eta]_{1''} + \lambda_4' [\eta^\dagger \eta]_{1''} [\eta \eta]_{1'} + \lambda_5 [\eta^\dagger \eta]_1 [\eta \eta]_1 + \lambda_6 \left([\eta^\dagger \eta]_{3_1} [\eta^\dagger \eta]_{3_1} + \text{h.c.} \right) \\
& + \lambda_7 [\eta^\dagger \eta]_{3_1} [\eta^\dagger \eta]_{3_2} + \lambda_8 [\eta^\dagger \eta]_{3_1} [\eta \eta]_{3_2} + \lambda_9 [\eta^\dagger \eta]_1 [H^\dagger H] + \lambda_{10} [\eta^\dagger H]_{3_1} [H^\dagger \eta]_{3_1} \\
& + \lambda_{11} \left([\eta^\dagger \eta]_1 H H + \text{h.c.} \right) + \lambda_{12} \left([\eta^\dagger \eta]_{3_1} [\eta H]_{3_1} + \text{h.c.} \right) + \lambda_{13} \left([\eta^\dagger \eta]_{3_1} [\eta^\dagger H]_{3_1} + \text{h.c.} \right) \\
& + \lambda_{14} \left([\eta^\dagger \eta]_{3_2} [\eta^\dagger H]_{3_1} + \text{h.c.} \right). \tag{6}
\end{aligned}$$

We assume that the couplings in the scalar potential are real and $\lambda_4 = \lambda_4'$ for simplicity. We note that this assumption means requiring CP conservation in the scalar potential. When one of the A_4 triplet field η_1 , in addition to H , has the VEV, the A_4 symmetry breaks to the subgroup Z_2 symmetry whose charge assignments are also shown in Table I. The Z_2 -even fields H and η_1 are defined as

$$H = \begin{pmatrix} \phi^+ \\ \frac{1}{\sqrt{2}}(v_h + \phi^0 + i\chi) \end{pmatrix}, \quad \eta_1 = \begin{pmatrix} w_1^+ \\ \frac{1}{\sqrt{2}}(v_\eta + \eta_{1R} + i\eta_{1I}) \end{pmatrix}. \tag{7}$$

Here the VEVs are real and satisfy $\sqrt{v_h^2 + v_\eta^2} = v = 246$ GeV. The stationary conditions are given by

$$\mu_H^2 + \lambda_1 v_h^2 + \frac{1}{2}(\lambda_9 + \lambda_{10} + 2\lambda_{11})v_\eta^2 = 0, \tag{8}$$

$$\mu_\eta^2 + (\lambda_2 + \lambda_3 + 2\lambda_4 + \lambda_5)v_\eta^2 + \frac{1}{2}(\lambda_9 + \lambda_{10} + 2\lambda_{11})v_h^2 = 0. \tag{9}$$

The physical scalar states in the Z_2 -even sector can be obtained by the mixing angles β , where $\tan \beta \equiv v_\eta/v_h$, and α as

$$\begin{pmatrix} G^+ \\ H^+ \end{pmatrix} = \begin{pmatrix} \cos \beta & \sin \beta \\ -\sin \beta & \cos \beta \end{pmatrix} \begin{pmatrix} \phi^+ \\ \omega_1^+ \end{pmatrix}, \quad \begin{pmatrix} G^0 \\ A_1 \end{pmatrix} = \begin{pmatrix} \cos \beta & \sin \beta \\ -\sin \beta & \cos \beta \end{pmatrix} \begin{pmatrix} \chi \\ \eta_{1I} \end{pmatrix}, \tag{10}$$

$$\begin{pmatrix} h_2 \\ h_1 \end{pmatrix} = \begin{pmatrix} \cos \alpha & \sin \alpha \\ -\sin \alpha & \cos \alpha \end{pmatrix} \begin{pmatrix} \phi^0 \\ \eta_{1R} \end{pmatrix}. \tag{11}$$

Here h_1 is the SM-like Higgs particle whose mass is $m_{h_1} = 125$ GeV. The masses of the charged scalar field H^\pm and the CP-odd scalar field A_1 are described as $m_{H^\pm}^2 = -\frac{1}{2}(\lambda_{10} + 2\lambda_{11})v^2$ and $m_{A_1}^2 = -2\lambda_{11}v^2$, respectively.

The Z_2 -odd fields η_2 and η_3 , which do not have VEVs, are defined as

$$\eta_2 = \begin{pmatrix} \eta_2^+ \\ \frac{1}{\sqrt{2}}(\eta_{2R} + i\eta_{2I}) \end{pmatrix}, \quad \eta_3 = \begin{pmatrix} \eta_3^+ \\ \frac{1}{\sqrt{2}}(\eta_{3R} + i\eta_{3I}) \end{pmatrix}. \quad (12)$$

These two states are mixed through the λ_{12} , λ_{13} , and λ_{14} terms in Eq. (6) and the mixing angle between them is $\pi/4$. The neutral CP-even (-odd) states give the mass eigenstates η_2^0 and η_3^0 (A_2 and A_3) with masses $m_{\eta_2^0}$ and $m_{\eta_3^0}$ (m_{A_2} and m_{A_3}) as

$$m_{\eta_2^0}^2 = \frac{1}{2} (\lambda_{x_1} v_\eta^2 - 3\lambda_{x_3} v_\eta v_h), \quad (13)$$

$$m_{\eta_3^0}^2 = \frac{1}{2} (\lambda_{x_1} v_\eta^2 + 3\lambda_{x_3} v_\eta v_h), \quad (14)$$

$$m_{A_2}^2 = \frac{1}{2} (\lambda_{x_2} v_\eta^2 - 4\lambda_{11} v_h^2 - \lambda_{x_3} v_\eta v_h), \quad (15)$$

$$m_{A_3}^2 = \frac{1}{2} (\lambda_{x_2} v_\eta^2 - 4\lambda_{11} v_h^2 + \lambda_{x_3} v_\eta v_h), \quad (16)$$

where $\lambda_{x_1} \equiv -3\lambda_3 - 6\lambda_4 + 2\lambda_6 + \lambda_7 + \lambda_8$, $\lambda_{x_2} \equiv -3\lambda_3 - 2\lambda_4 - 4\lambda_5 - 2\lambda_6 + \lambda_7 + \lambda_8$ and $\lambda_{x_3} \equiv \lambda_{12} + \lambda_{13} + \lambda_{14}$. The masses of the charged scalar fields η_2^\pm and η_3^\pm are given by

$$m_{\eta_2^\pm}^2 = \frac{1}{2} [\lambda_{x_4} v_\eta^2 + (\lambda_{10} + \lambda_{11}) v_h^2 - \lambda_{x_3} v_h v_\eta], \quad (17)$$

$$m_{\eta_3^\pm}^2 = \frac{1}{2} [\lambda_{x_4} v_\eta^2 + (\lambda_{10} + \lambda_{11}) v_h^2 + \lambda_{x_3} v_h v_\eta], \quad (18)$$

where $\lambda_{x_4} \equiv -3\lambda_3 - 4\lambda_4 - 2\lambda_5 + \lambda_8$. Note that the mass differences between $m_{\eta_2^0}$ and $m_{\eta_3^0}$, m_{A_2} and m_{A_3} , $m_{\eta_2^\pm}$ and $m_{\eta_3^\pm}$ are given by λ_{x_3} .

The lightest Z_2 -odd particle is stable and can be a DM if it is neutral. In our model, the right-handed neutrinos are heavy as shown later, so that the DM candidates are $\eta_{2,3}^0$ and $A_{2,3}$. Hereafter, we assume that η_2^0 is a DM candidate.

III. NEUTRINO MASSES AND FLAVOR STRUCTURES

In this model, the neutrinos obtain their masses via the tree-level and the one-loop seesaw mechanisms. Since the Yukawa interactions $L_\alpha \tilde{H} N_i$ ($\alpha = e, \mu, \tau$) are forbidden by the A_4 symmetry, the usual Type-I seesaw mechanism does not work. However, the neutrinos can obtain their masses via the other tree-level seesaw mechanism due to the existence of the Yukawa interactions $L_\alpha \tilde{\eta}_1 N_1$ in Eq. (4) with the non-zero VEV of η_1 . The neutrino mass matrix M_ν^{tree} that is generated by the tree-level seesaw mechanism in Fig. 1 is given by

$$M_\nu^{\text{tree}} = \frac{v_\eta^2}{2M_1} \begin{pmatrix} y & 0 & 0 \\ y & 0 & 0 \\ y & 0 & 0 \end{pmatrix} \begin{pmatrix} y & y & y \\ 0 & 0 & 0 \\ 0 & 0 & 0 \end{pmatrix} = \frac{v_\eta^2 y^2}{2M_1} \begin{pmatrix} 1 & 1 & 1 \\ 1 & 1 & 1 \\ 1 & 1 & 1 \end{pmatrix}. \quad (19)$$

The flavor structure in M_ν^{tree} is the same form as that of the b term in Eq. (3).⁵ We note that the rank of M_ν^{tree} is one, so that other contributions to the neutrino mass generation should be necessary.

The neutrino masses are also generated by the one-loop seesaw mechanisms that are shown in Figs. 2 and 3. The Z_2 -even right-handed neutrino N_1 contributes to the mass generation in Fig. 2, while the Z_2 -odd right-handed neutrinos N_2 , N_3 and their mixing contribute in Fig. 3. Assuming $\lambda_{x_3} \ll 1$ and $\sin(\beta - \alpha) = 1$, where the former assumption leads to $m_\eta \equiv m_{\eta_2^0} \approx m_{\eta_3^0}$ and $m_A \equiv m_{A_2} \approx m_{A_3}$, the neutrino mass matrix via the one-loop diagrams in Figs. 2 and 3 is described as

$$\begin{aligned}
M^{\text{one-loop}} &= \begin{pmatrix} 1 & 1 & 1 \\ 1 & \omega & \omega^2 \\ 1 & \omega^2 & \omega \end{pmatrix} \begin{pmatrix} 1 & 0 & 0 \\ 0 & \cos \hat{\theta}_R & \sin \hat{\theta}_R \\ 0 & -\sin \hat{\theta}_R & \cos \hat{\theta}_R \end{pmatrix} \begin{pmatrix} \Lambda_1 & 0 & 0 \\ 0 & \Lambda_2 & 0 \\ 0 & 0 & \Lambda_3 \end{pmatrix} \begin{pmatrix} 1 & 0 & 0 \\ 0 & \cos \hat{\theta}_R & -\sin \hat{\theta}_R \\ 0 & \sin \hat{\theta}_R & \cos \hat{\theta}_R \end{pmatrix} \begin{pmatrix} 1 & 1 & 1 \\ 1 & \omega & \omega^2 \\ 1 & \omega^2 & \omega \end{pmatrix} \\
&= X_a \begin{pmatrix} 1 & 0 & 0 \\ 0 & 1 & 0 \\ 0 & 0 & 1 \end{pmatrix} + \left[\Lambda_1 - \frac{X_a + X_c + X_d}{3} \right] \begin{pmatrix} 1 & 1 & 1 \\ 1 & 1 & 1 \\ 1 & 1 & 1 \end{pmatrix} + X_c \begin{pmatrix} 1 & 0 & 0 \\ 0 & 0 & 1 \\ 0 & 1 & 0 \end{pmatrix} + X_d \begin{pmatrix} 0 & 0 & 1 \\ 0 & 1 & 0 \\ 1 & 0 & 0 \end{pmatrix}.
\end{aligned} \tag{20}$$

Here

$$\Lambda_1 \equiv \frac{y^2 M_1}{16\pi^2} \left[\sin^2 \beta \frac{m_{h_1}^2}{m_{h_1}^2 - M_1^2} \ln \frac{m_{h_1}^2}{M_1^2} + \cos^2 \beta \left(\frac{m_{h_2}^2}{m_{h_2}^2 - M_1^2} \ln \frac{m_{h_2}^2}{M_1^2} - \frac{m_{A_1}^2}{m_{A_1}^2 - M_1^2} \ln \frac{m_{A_1}^2}{M_1^2} \right) \right], \tag{21}$$

$$\Lambda_k \equiv \frac{y^2 M_k e^{\delta_{R_k}}}{16\pi^2} \left[\frac{m_\eta^2}{m_\eta^2 - M_k^2} \ln \frac{m_\eta^2}{M_k^2} - \frac{m_A^2}{m_A^2 - M_k^2} \ln \frac{m_A^2}{M_k^2} \right] \quad (k = 2, 3), \tag{22}$$

$$X_a \equiv 3 \cos \hat{\theta}_R \sin \hat{\theta}_R (\Lambda_3 - \Lambda_2), \tag{23}$$

$$X_c \equiv \left[(1 - \omega)(\Lambda_2 \cos^2 \hat{\theta}_R + \Lambda_3 \sin^2 \hat{\theta}_R) + (1 - \omega^2)(\Lambda_2 \sin^2 \hat{\theta}_R + \Lambda_3 \cos^2 \hat{\theta}_R) \right], \tag{24}$$

$$X_d \equiv \left[(\omega^2 - \omega)(\Lambda_2 \cos^2 \hat{\theta}_R + \Lambda_3 \sin^2 \hat{\theta}_R) + (\omega - \omega^2)(\Lambda_2 \sin^2 \hat{\theta}_R + \Lambda_3 \cos^2 \hat{\theta}_R) \right]. \tag{25}$$

It can be seen that the four flavor structures in Eq. (3) are generated.⁶ We find that the one-loop diagrams with N_1 in Fig. 2 generate only the b term. On the other hand, the contributions of

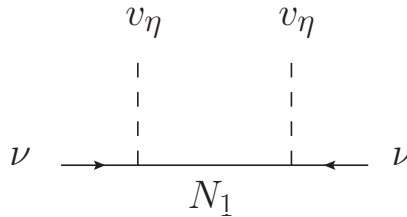


FIG. 1. Feynman diagram for neutrino mass via the tree-level seesaw mechanism.

⁵ It is noted that when the A_4 symmetry is broken to the Z_3 symmetry via $\langle \eta \rangle = (v_\eta, v_\eta, v_\eta)$, the b , c , and d terms are generated by the tree-level seesaw mechanism.

⁶ Even when the assumption $\lambda_{x_3} \ll 1$ is removed, the four flavor structures are derived.

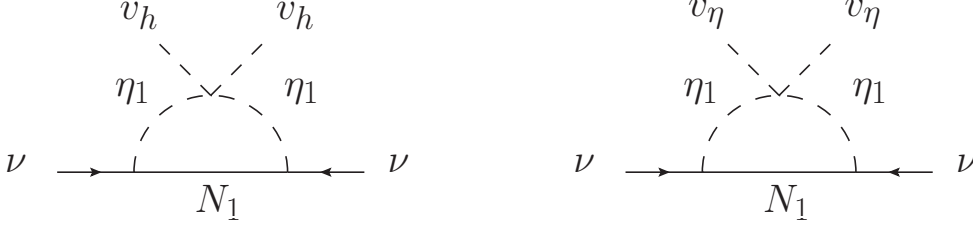


FIG. 2. Feynman diagrams for neutrino masses via the one-loop seesaw mechanism with N_1 .

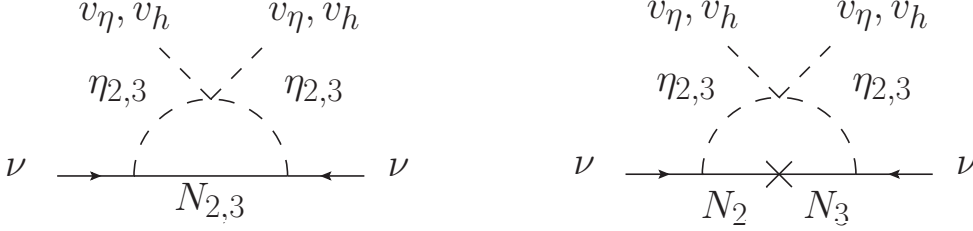


FIG. 3. Feynman diagrams for neutrino masses via the one-loop seesaw mechanism with N_2 and N_3 .

N_2 and N_3 in Fig. 3 give all four flavor structures. In particular, the mixing between N_2 and N_3 realizes the non-zero a term, while the origin of the non-zero d term (*i.e.*, non-zero θ_{13}) comes from the difference between Λ_2 and Λ_3 . From Eqs. (19) and (20), the neutrino mass matrix in our model is given by

$$\begin{aligned}
M_\nu &= M_\nu^{\text{tree}} + M^{\text{one-loop}} \\
&= X_a \begin{pmatrix} 1 & 0 & 0 \\ 0 & 1 & 0 \\ 0 & 0 & 1 \end{pmatrix} + \left[\frac{v_\eta^2 y^2}{2M_1} + \Lambda_1 - \frac{X_a + X_c + X_d}{3} \right] \begin{pmatrix} 1 & 1 & 1 \\ 1 & 1 & 1 \\ 1 & 1 & 1 \end{pmatrix} + X_c \begin{pmatrix} 1 & 0 & 0 \\ 0 & 0 & 1 \\ 0 & 1 & 0 \end{pmatrix} + X_d \begin{pmatrix} 0 & 0 & 1 \\ 0 & 1 & 0 \\ 1 & 0 & 0 \end{pmatrix},
\end{aligned} \tag{26}$$

where the flavor structures are the same as those in Eq. (3). In this model, the ratios $|b|/|c|$ and $|b|/|d|$ are naively given by the inverse of the loop suppression factor $\approx 16\pi^2$ when $M_i \sim m_\eta$, since the b term contains the contributes from the tree-level diagrams whereas the c and d terms are generated by the one-loop diagrams. However, such large hierarchies between b and c , d are not plausible with the current experimental data, as will be shown later. On the other hand, when $M_i \gg m_\eta$, we obtain $M_\nu^{\text{tree}}/\Lambda_i \propto 16\pi^2 \left[\ln \frac{M_i^2}{m_\eta^2} - 1 \right]^{-1}$. As the mass difference between M_i and m_η becomes larger, the ratio $M_\nu^{\text{tree}}/\Lambda_i$ becomes smaller. Therefore, milder (but large) hierarchies between b and c , d , such as $|b|/|c| \sim |b|/|d| \sim \mathcal{O}(10)$, can be possible. For the a term, although it is also generated by the one-loop diagrams, its magnitude is controlled by the mixing between N_2 and N_3 .

The neutrino mass matrix in Eq. (3) (and thus in Eq. (26)) is diagonalized with the PMNS matrix that is formed by the tri-bimaximal mixing, the (1,3) mixing and the Majorana phase

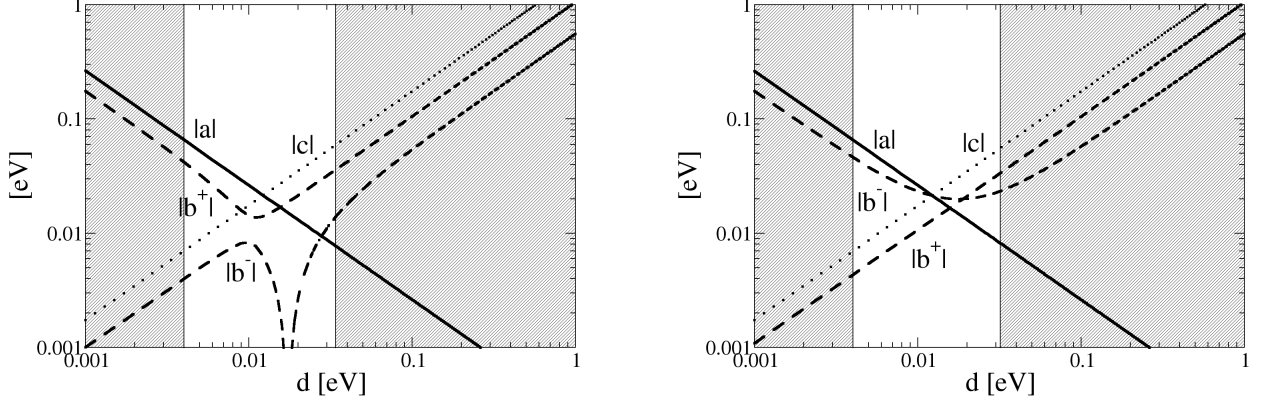


FIG. 4. The coefficients of the flavor structure $|a|$, $|b|$, and $|c|$ as a function of d for the NO (left panel) and the IO (right panel). The values of the neutrino oscillation parameters are taken as in Eq. (32) with $\delta = 0$. The shaded regions are excluded by the constraint of the sum of light neutrino masses [49].

matrix [29]:

$$U_{\text{PMNS}} = \begin{pmatrix} \frac{2}{\sqrt{6}} & \frac{1}{\sqrt{3}} & 0 \\ -\frac{1}{\sqrt{6}} & \frac{1}{\sqrt{3}} & -\frac{1}{\sqrt{2}} \\ -\frac{1}{\sqrt{6}} & \frac{1}{\sqrt{3}} & \frac{1}{\sqrt{2}} \end{pmatrix} \begin{pmatrix} \cos \hat{\theta} & 0 & \sin \hat{\theta} \\ 0 & 1 & 0 \\ -\sin \hat{\theta} & 0 & \cos \hat{\theta} \end{pmatrix} \begin{pmatrix} 1 & 0 & 0 \\ 0 & e^{i\alpha_2/2} & 0 \\ 0 & 0 & e^{i\alpha_3/2} \end{pmatrix}. \quad (27)$$

Here the mixing angle $\hat{\theta}$ is the complex parameter. Comparing this to the standard parametrization of U_{PMNS} in Eq. (1), we obtain $\sin \hat{\theta} = \sqrt{3/2} \sin \theta_{13} e^{-i\delta}$. Using the coefficient parameters a , b , c , and d in Eq. (3), the angle $\hat{\theta}$ is given by

$$\tan 2\hat{\theta} = \frac{\sqrt{3}d}{-2c + d}. \quad (28)$$

The neutrino masses m_1 , m_2 , and m_3 and the Majorana phases α_2 and α_3 are written as

$$m_1 = \left| a + \sqrt{c^2 + d^2 - cd} \right|, \quad m_2 = |a + 3b + c + d|, \quad m_3 = \left| a - \sqrt{c^2 + d^2 - cd} \right|, \quad (29)$$

$$\alpha_2 = \arg(a + 3b + c + d) - \arg\left(a + \sqrt{c^2 + d^2 - cd}\right), \quad (30)$$

$$\alpha_3 = \arg\left(a - \sqrt{c^2 + d^2 - cd}\right) - \arg\left(a + \sqrt{c^2 + d^2 - cd}\right). \quad (31)$$

The observed values of the neutrino oscillation parameters Δm_{31}^2 , Δm_{21}^2 , θ_{13} and δ give constraints on the relationship between the coefficients a , b , c , and d .

In Fig. 4, we show the absolute values of the coefficients $|a|$ (solid lines), $|b|$ (dashed lines) and $|c|$ (dotted lines) as a function of d that is assumed to be real and positive, for the NO (left panel) and the IO (right panel). The coefficients are derived from the following center values in the NO

(IO) [19]:⁷

$$\Delta m_{21}^2 = 7.39 \times 10^{-5} \text{ eV}^2, \quad \Delta m_{31}^2 = 2.525 (-2.512) \times 10^{-3} \text{ eV}^2, \quad \theta_{13} = 8.61 (8.65)^\circ. \quad (32)$$

The Dirac phase is taken as $\delta = 0$ and the coefficients a , b , and c are assumed to be real for simplicity. There are two solutions for $|b|$, which are shown by $|b^+|$ and $|b^-|$ in Fig. 4. The shaded regions are excluded by the constraint of the sum of light neutrino masses using the Planck TT, TE, EE+lowE+lensing [49]:

$$\sum_i m_i < 0.241 \text{ eV}. \quad (33)$$

In the NO (left panel of Fig. 4), $|a|$ decreases and $|c|$ increases as the parameter d becomes larger. We note that the coefficients $|c|$ and $|d|$ are comparable but $|c|$ is larger than $|d|$ due to the relation of Eq. (28). The hierarchy $|a|, |b^+| > |c|, |d|$ is shown for the smaller d ($d \lesssim 0.008 \text{ eV}$), while the hierarchy $|b^+|, |c|, |d| > |a|$ appears for the larger d ($d \gtrsim 0.02 \text{ eV}$). On the other hand, the hierarchy $|a|, |c|, |d| > |b^-|$ is obtained for $d \sim 0.03 \text{ eV}$, where b^- changes its sign. In the IO (right panel), similar hierarchies among the coefficients can be seen except for the disappearance of $|b^-|$.⁸ We note that, in both the NO and the IO, the large hierarchies between b and c , d such as $|b|/|c|$, $|b|/|d| \approx 16\pi^2$ are disfavored by current data.

In our hybrid seesaw model, the milder but large hierarchy of $|b|/|d| \approx \pi^2$ can be realized for $M_i \gg m_\eta$ as mentioned in the previous section. In the following, we give the benchmark point in the NO (BP_{NO}) and the IO (BP_{IO}), respectively, where the ratio $|b|/|d| \approx \pi^2$ is satisfied. Here we take the coefficients a , b , c , and d as complex parameters and take into account the contributions of CP phases. For BP_{NO}, we take the following set for a , b , c , and d , which satisfies the center values of the neutrino parameters in Eq. (32) and $\delta = 222^\circ$ [19]:

$$\begin{aligned} |a| &\approx 0.0759 \text{ eV}, \quad |b| \approx 0.0483 \text{ eV}, \quad |c| \approx 0.0103 \text{ eV}, \quad |d| \approx 0.0045 \text{ eV}, \\ \arg(a) &\approx 2.45 \text{ rad}, \quad \arg(b) \approx -0.439 \text{ rad}, \quad \arg(c) \approx 2.09 \text{ rad}, \quad \arg(d) \approx 1.44 \text{ rad} \end{aligned} \quad (34)$$

The above set is realized by the following values of the model parameters:

$$\begin{aligned} \tan \beta &= 3, \quad y = 1.0 \times 10^{-2}, \quad (M_1, M_2, M_3) \approx (6.69, 1.94, 1.53) \times 10^{10} \text{ GeV} \\ \delta_{R_2} &\approx -0.66 \text{ rad}, \quad \delta_{R_3} \approx 2.43 \text{ rad}, \quad \tan 2\hat{\theta}_R \approx -16.5 + 10.4i, \\ m_{h_2} &= 200 \text{ GeV}, \quad m_{A_1} = 250 \text{ GeV}, \quad m_\eta = 500 \text{ GeV}, \quad m_A = 520 \text{ GeV}. \end{aligned} \quad (35)$$

For the IO, we take the following set for the BP_{IO}, which satisfies Eq. (32) and $\delta = 285^\circ$ [19]:

$$\begin{aligned} |a| &\approx 0.0707 \text{ eV}, \quad |b| \approx 0.0536 \text{ eV}, \quad |c| \approx 0.00978 \text{ eV}, \quad |d| \approx 0.0049 \text{ eV}, \\ \arg(a) &\approx 0.063 \text{ rad}, \quad \arg(b) \approx 3.14 \text{ rad}, \quad \arg(c) \approx 0.044 \text{ rad}, \quad \arg(d) \approx -1.51 \text{ rad} \end{aligned} \quad (36)$$

⁷ We use the center values in v4.1 of Ref. [19].

⁸ In the left panel of Fig. 4, b^+ is positive (*i.e.*, $\arg(b^+) = 0$), b^- is positive for $d < 0.02 \text{ eV}$ and negative (*i.e.*, $\arg(b^-) = \pi \text{ rad}$) for $d > 0.02 \text{ eV}$, and a and c are negative. In the right panel of Fig. 4, a , b^+ , b^- , and c are positive, positive, negative, and negative, respectively.

The above set is realized by the following:

$$\begin{aligned}\tan\beta &= 3, \quad y = 1.0 \times 10^{-2}, \quad (M_1, M_2, M_3) \approx (6.02, 2.16, 1.61) \times 10^{10} \text{ GeV} \\ \delta_{R_2} &\approx -3.12 \text{ rad}, \quad \delta_{R_3} \approx 0.091 \text{ rad}, \quad \tan 2\hat{\theta}_R \approx -16.7, \\ m_{h_2} &= 200 \text{ GeV}, \quad m_{A_1} = 250 \text{ GeV}, \quad m_\eta = 500 \text{ GeV}, \quad m_A = 520 \text{ GeV}.\end{aligned}\tag{37}$$

From Eqs. (35) and (37), we find that the large hierarchy $|b|/|d| \approx \pi^2$ is realized for the masses of the right-handed neutrinos $M_i \sim \mathcal{O}(10^{10})$ GeV and the scalar fields $m_{\eta_i} \sim \mathcal{O}(10^{2-3})$ GeV for $y \sim 10^{-2}$. Furthermore, both the BP_{NO} and the BP_{IO} satisfy $|a| \gg |c|, |d|$, so that the Majorana phase α_3 is expected to be close to zero, as can be seen from Eq. (31).

IV. PREDICTIONS OF THE EFFECTIVE NEUTRINO MASS AND THE MAJORANA PHASES

In this section, we discuss the predictions of the effective neutrino mass m_{ee} and the Majorana CP phases. m_{ee} is defined as

$$m_{ee} = \left| \sum_{i=1}^3 U_{ei}^2 m_i \right| \tag{38}$$

with $U_{e1} = 2\cos\hat{\theta}/\sqrt{6}$, $U_{e2} = 1/\sqrt{3}$, and $U_{e3} = 2\sin\hat{\theta}/\sqrt{6}$. First, we show the results of the model-independent analysis by using the neutrino mass matrix in Eq. (3), focusing on the hierarchies between the coefficients a , b , c , and d . In Figs. 5 and 6, the predicted values of m_{ee} are shown as functions of the lightest neutrino mass (upper panel) and the Majorana phases α_2 (lower left panel) and α_3 (lower right panel) for the NO and the IO, respectively. In these plots, we have taken the following ranges for the coefficient parameters $|d|$, $\arg(a)$, $\arg(b)$, $\arg(d)$, and the 3σ range of δ in the NO (IO) [19]:

$$\begin{aligned}0 \leq |d|/\text{eV} \leq 1.0, \quad 0 \leq \arg(a)/\text{rad} < 2\pi, \quad 0 \leq \arg(b)/\text{rad} < 2\pi, \\ 0 \leq \arg(d)/\text{rad} < 2\pi, \quad 107^\circ \leq \delta \leq 403^\circ \quad (192^\circ \leq \delta \leq 360^\circ).\end{aligned}\tag{39}$$

The other parameters $|a|, |b|, |c|$ can be determined so as to satisfy the observed values of Δm_{21}^2 , Δm_{31}^2 and θ_{13} in Eq. (32). Furthermore, $\arg(c)$ is fixed through the relation in Eq. (28). In Figs. 5 and 6, the cyan points show all points that satisfy the observed values in Eq. (32) and the constraint from Eq. (33). The green, black, orange and yellow points show the result where the hierarchical conditions $|b|/|d| > 1$, $|b|/|a| > 1$, $|d|/|a| > 1$, and $|b|/|c| > 1$, respectively, are further imposed. The horizontal blue solid and dashed lines show the upper bound on m_{ee} by the global fit of neutrinoless double beta decay ($0\nu\beta\beta$) experiments $m_{ee} \lesssim 0.06$ eV [19] and the sensitivity of the next-generation $0\nu\beta\beta$ experiment by nEXO [50].

In Fig. 5, the hierarchical case with $|b|/|d| > 1$ (green) does not constrain the parameter space compared to the cyan points, while the other three cases constrain the parameter space. For the

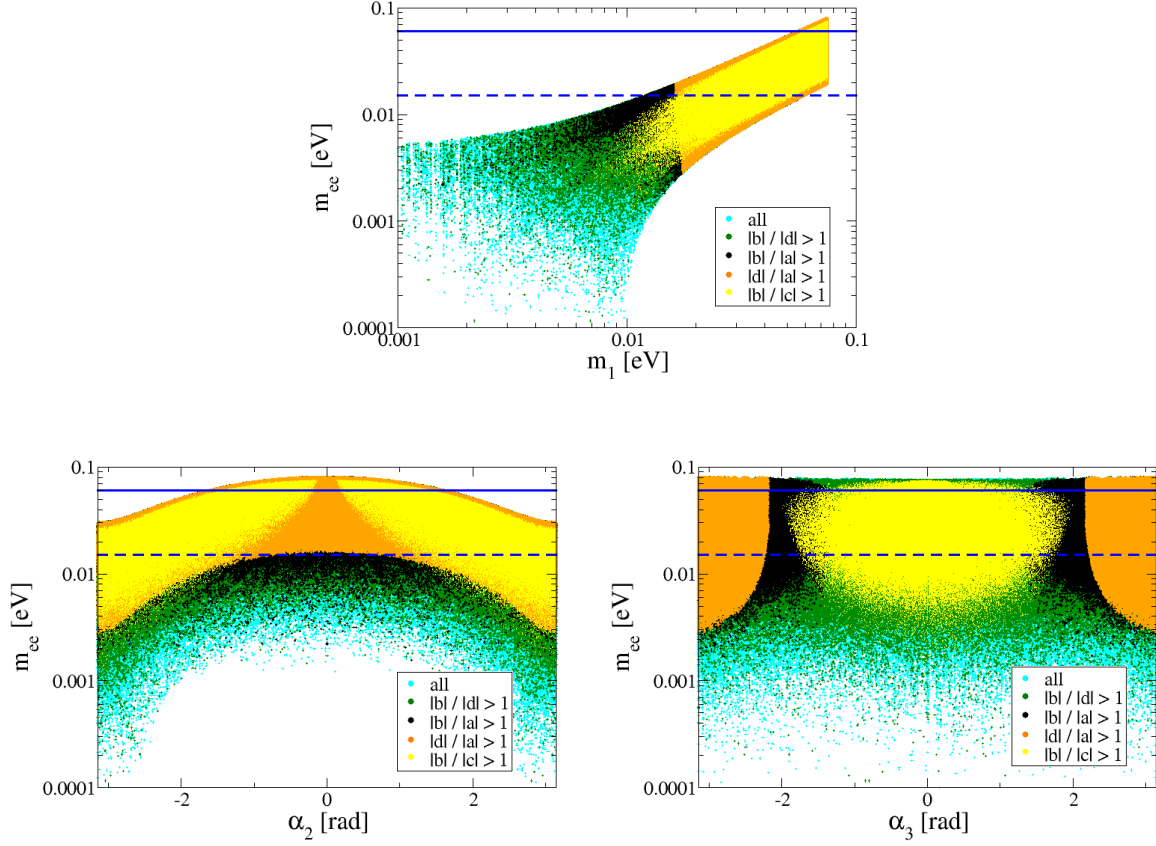


FIG. 5. m_{ee} versus m_1 (upper panel), α_2 (lower left panel), α_3 (lower right panel) for the NO. The cyan points show all points that satisfy Eqs. (32) and (33), the green, black, orange, and yellow points show respectively the hierarchy case with $|b|/|d| > 1$, $|b|/|a| > 1$, $|d|/|a| > 1$, and $|b|/|c| > 1$.

hierarchical case with $|b|/|c| > 1$ (yellow), the predicted regions of the effective neutrino mass m_{ee} and the lightest neutrino mass m_1 are $m_{ee} \gtrsim 0.001$ eV and $m_1 \gtrsim 0.007$ eV. In this case, the Majorana phase $\alpha_2 \sim 0$ is excluded by the constraint from Eq. (33) and α_3 is constrained as $|\alpha_3|/\text{rad} \lesssim 2.0$. The hierarchical cases with $|d|/|a| > 1$ (orange) and $|b|/|a| > 1$ (black) have similar predictions, but the former is more constrained, such as giving $m_1 \gtrsim 0.015$ eV and $|\alpha_3|/\text{rad} \gtrsim 2.2$. Here $|\alpha_3| \simeq \pi$ radians are obtained for $|d| \gg |a|$ as can be seen from Eq. (31). Figure 6 shows the results for the IO. For the hierarchical case with $|b|/|c| > 1$, the predicted regions for m_3 and α_3 are wider than those in the NO. In particular, α_3 is not constrained for $0.015 \lesssim m_{ee}/\text{eV} \lesssim 0.04$. Similarly, in that range of m_{ee} , α_3 is unconstrained for the case with $|b|/|a| > 1$ (although this is not shown in the lower right panel in Fig. 6 as it is behind the yellow region). The predictions for the cases with $|d|/|a| > 1$ show similar features to those in the NO. The next-generation $0\nu\beta\beta$ experiment nEXO can explore all predicted regions of m_{ee} for the IO, and thus there is the possibility of obtaining hints to the Majorana phases for some hierarchical cases. In this analysis,

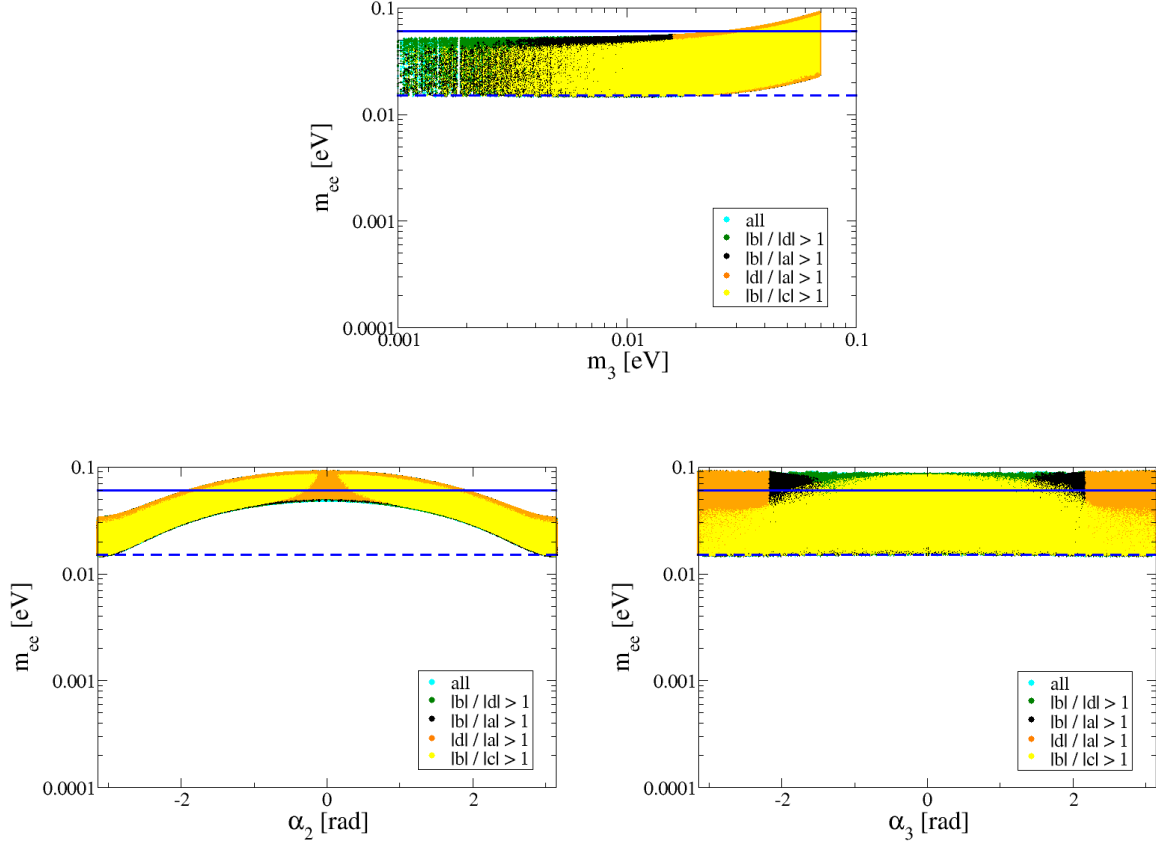


FIG. 6. Same as Fig. 5 except for the IO and the lightest neutrino mass m_3 .

the predicted values for θ_{23} and θ_{12} are $0.4 \lesssim \sin^2 \theta_{23} \lesssim 0.6$ and $\sin^2 \theta_{12} \approx 0.34$, respectively, which are allowed within 3σ [19]. We note that the predicted regions of the hierarchies with $|b|/|c| > 1$ and $|d|/|a| > 1$ are included in those with $|b|/|d| > 1$ and $|c|/|a| > 1$, respectively, because of the relation $|c| > |d|$ obtained by Eq. (28).

Next, we discuss the larger hierarchical case with $|b|/|d| > \pi^2$ that can be applied to our model. We display in Figs. 7 and 8 the predictions of m_{ee} for $|b|/|d| > \pi^2$ by the red points. The green points are the predictions for $|b|/|d| > 1$ that are the same as those in Figs. 5 and 6. We also show the predictions of the BP_{NO} and the BP_{IO} in our hybrid seesaw model by the black triangles in Figs. 7 and 8, respectively. In Fig. 7, we can see that the predicted regions for $|b|/|d| > \pi^2$ are strictly constrained : $m_{ee} \gtrsim 0.02$ eV, $m_1 \gtrsim 0.06$ eV, $\pi/2 \lesssim |\alpha_2|/\text{rad} \leq \pi$, $|\alpha_3|/\text{rad} \lesssim 0.2$. Such large m_{ee} is within the sensitivity reach of the next-generation $0\nu\beta\beta$ experiments. Note that, for the larger hierarchy between the coefficients $|b|$ and $|d|$, a larger hierarchy between $|a|$ and $|d|$ is expected and thus the Majorana phase $|\alpha_3|$ gets closer to zero. In our hybrid seesaw model, the predicted values of the BP_{NO} are:

$$m_{ee} \approx 0.030 \text{ eV}, m_1 \approx 0.067 \text{ eV}, \alpha_2 \approx -2.5 \text{ rad}, \alpha_3 \approx -0.07 \text{ rad} \quad (40)$$

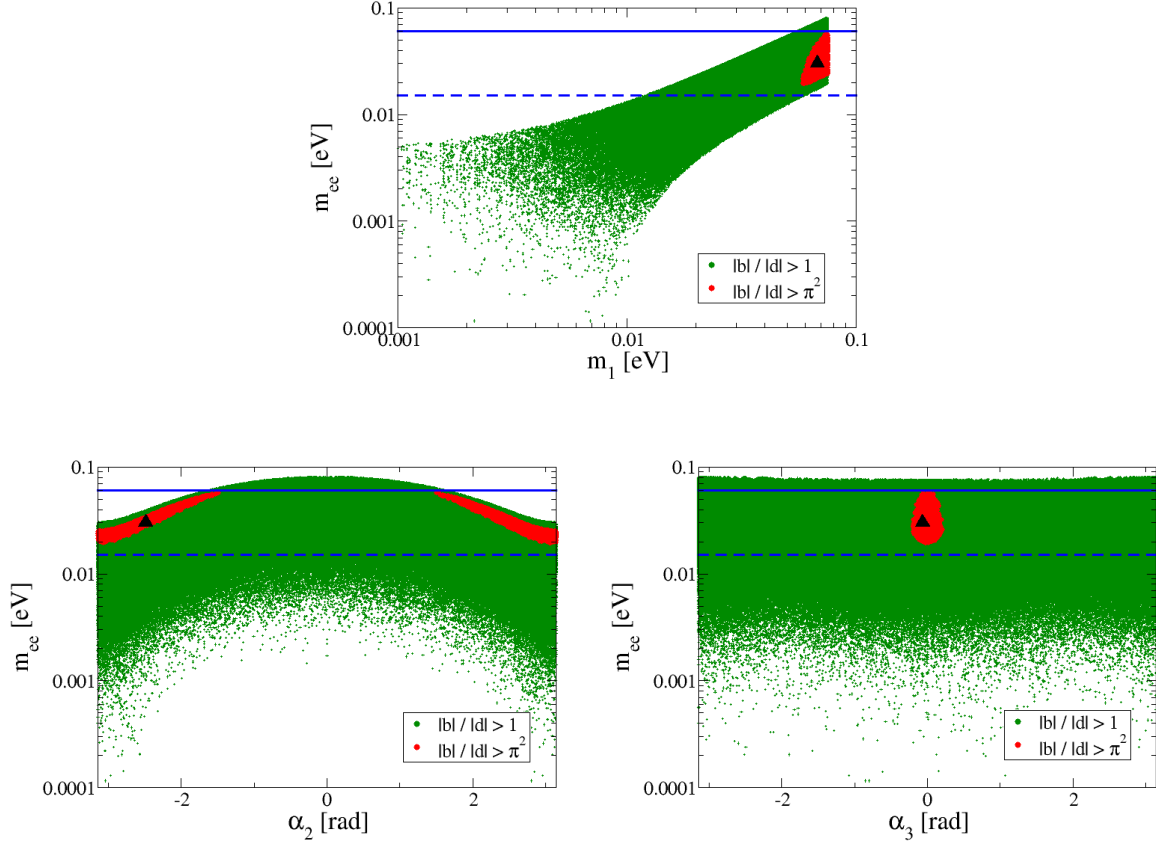


FIG. 7. m_{ee} versus m_1 (upper panel), α_2 (lower left panel), α_3 (lower right panel) for the NO. The green points are the same as those in Fig. 5. The red points show the large hierarchy case, $|b|/|d| > \pi^2$: the black triangle point indicates the BP_{NO} .

Figure 8 shows the results for the IO, where we can see similar predictions for the red regions with the NO. The predicted values of the BP_{IO} are:

$$m_{ee} \approx 0.027 \text{ eV}, \quad m_3 \approx 0.061 \text{ eV}, \quad \alpha_2 \approx 3.04 \text{ rad}, \quad \alpha_3 \approx -0.07 \text{ rad}, \quad (41)$$

where the non-significant CP violations by the Majorana phases are expected.

V. DARK MATTER

The A_4 flavor symmetry in our model is spontaneously broken to the Z_2 symmetry via the VEV of the A_4 triplet scalar field, which predicts the DM candidates and we assume that the Z_2 -odd scalar field η_2^0 is the DM.⁹ The main annihilation processes of the DM in our scenario are shown in Fig. 9. Note that the processes are almost the same as those in the inert doublet model [56].¹⁰

⁹ Such DM (so-called “discrete DM”) is discussed in Refs. [38, 39, 48, 51–55].

¹⁰ The scalar fields η_2^0 , η_3^0 , A_2 and A_3 can be probed at the collider experiments via the processes that are similar to the inert doublet model [56–58].

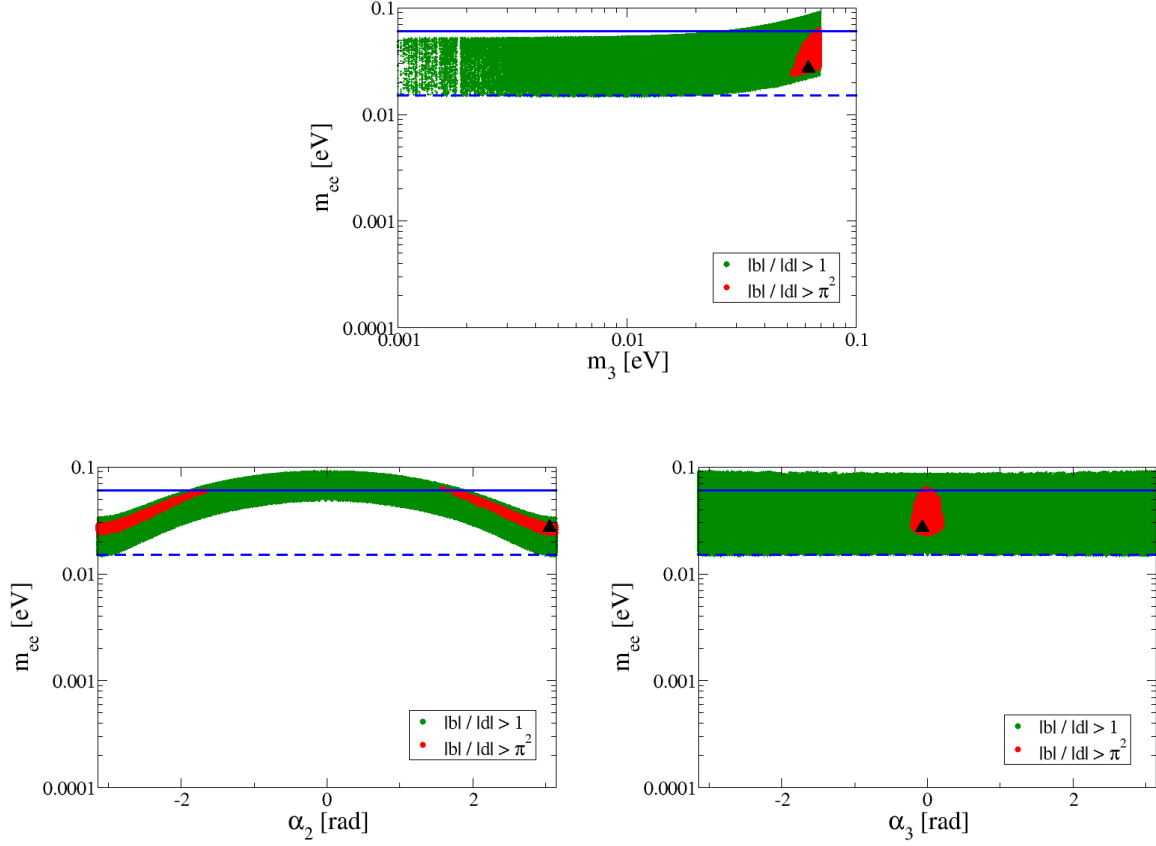


FIG. 8. Same as Fig. 7 except for the IO and the lightest neutrino mass m_3 .

In our model, the mass splitting between η_2^0 and η_3^0 is small because of the small λ_{x_3} coupling, so that we also consider the annihilation of η_3^0 and the relic density is computed for the sum of η_2^0 and η_3^0 .¹¹ The rate of DM annihilation depends on the scalar couplings λ_1 , λ_{x_5} , λ_{x_6} , and λ_{x_7} , except for the gauge couplings, where $\lambda_{x_5} \equiv \lambda_9 + \lambda_{10} + 2\lambda_{11}$, $\lambda_{x_6} \equiv \lambda_2 + \lambda_3 + 2\lambda_4 + \lambda_5$, and $\lambda_{x_7} \equiv 2\lambda_2 - \lambda_3 - 2\lambda_4 + \lambda_5 + 2\lambda_6 + \lambda_7 + \lambda_8$. For $\sin(\beta - \alpha) = 1$, the relevant scalar couplings λ_{x_5} , λ_{x_6} , and λ_1 are given by the masses of the Z_2 -even neutral scalar fields m_{h_1} , m_{h_2} and the mixing angle β as

$$\lambda_{x_5} = \frac{m_{h_1}^2 - m_{h_2}^2}{v^2 [\sin^2 \beta + \cos^2 \beta (1 + 2 \sin 2\beta)]}, \quad (42)$$

$$\lambda_{x_6} = \frac{m_{h_2}^2}{v^2 \sin^2 \beta} + \lambda_{x_5}, \quad (43)$$

$$\lambda_1 = \frac{\lambda_{x_5} \cos 2\beta + \lambda_{x_6} \sin^2 \beta}{\cos^2 \beta}. \quad (44)$$

The scalar coupling λ_{x_7} can be determined to satisfy the relic abundance $\Omega h^2 \approx 0.12$ [49].

¹¹ We note that η_3^0 decays into η_2^0 through, *e.g.*, $\eta_3^0 \rightarrow \eta_2^0 \gamma$ after its decoupling.

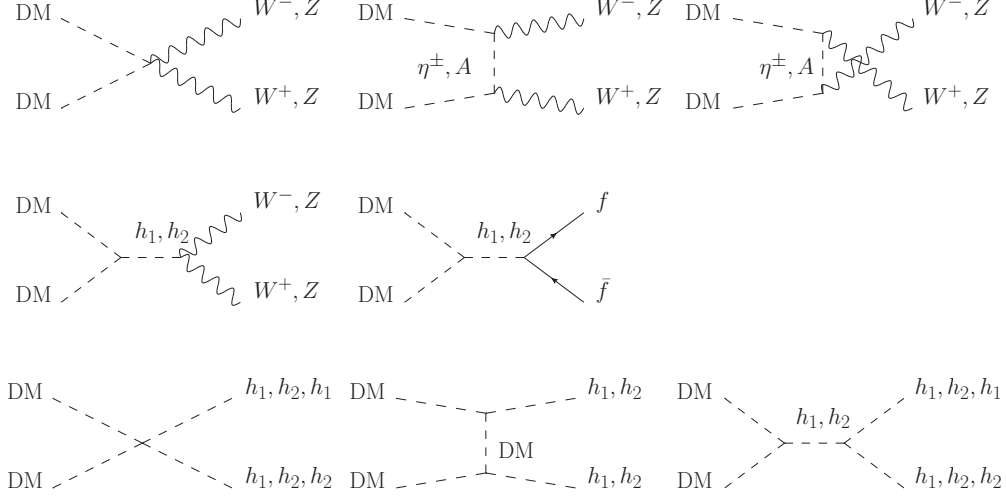


FIG. 9. Feynman diagrams giving main contributions to the relic abundance.

The spin-independent cross section of the nucleon is given by

$$\sigma_{\text{SI}} = \frac{1}{\pi} \left(\frac{\lambda_{\text{DD}} \hat{f} m_N}{m_{\eta_2^0} m_{h_1}^2} - \frac{\lambda'_{\text{DD}} \hat{f} m_N}{m_{\eta_2^0} m_{h_2}^2 \tan \beta} \right)^2 \left(\frac{m_N m_{\eta_2^0}}{m_N + m_{\eta_2^0}} \right)^2, \quad (45)$$

where $\hat{f} \approx 0.3$ is the usual nucleonic matrix element [59], m_N is the nucleon mass, $\lambda_{\text{DD}} = \lambda_{x_7} \sin^2 \beta + \lambda_{x_5} \cos^2 \beta$, and $\lambda'_{\text{DD}} = \lambda_{x_7} \sin 2\beta - \lambda_{x_5} \sin 2\beta$. Since the contributions from the h_1 and h_2 mediations give a relative negative sign, there is a possibility of destructive interference for $m_{h_1} \sim m_{h_2}$.

In Fig. 10, the spin-independent cross section of DM is shown as a function of the DM mass, where the relic abundance of the DM satisfies $\Omega h^2 \approx 0.12$ [49]. Here we have fixed the masses of the Z_2 -even scalar fields as $m_{h_2} = 200$ GeV and $m_{H^\pm} = m_{A_1} = 250$ GeV. For the Z_2 -odd scalar fields, the masses are taken as $m_A = m_{\eta^\pm} = m_{\eta^0} + 20$ GeV. The cyan, red, blue and green lines show the results for $\tan \beta = 1, 2, 3$, and 4 , respectively, where the dotted lines are excluded by the unitarity condition $\lambda_i < 4\pi$ ($i = 1 - 14$) or the bounded-from-below condition on the scalar potential [48]. As a reference, we show the prediction of the BP_{NO} and the BP_{IO} by a black triangle. The region above the black dashed line is excluded by XENON1T [60]. In Fig. 10, we can see the cancellations between the contributions of h_1 and h_2 . When the DM mass is smaller than about 400 GeV, the relic abundance of the DM is smaller than the observed value $\Omega h^2 < 0.12$. For $\tan \beta \gtrsim 5$, the unitarity condition cannot be satisfied. We find that the allowed ranges for the DM mass are $m_{\eta_2^0} \simeq 520 - 540$ GeV, $490 - 580$ GeV, and $400 - 500$ GeV for $\tan \beta = 2, 3$, and 4 , respectively. The future sensitivity of the direct detection experiment XENONnT is $\sigma_{\text{SI}} \sim \mathcal{O}(10^{-47}) \text{ cm}^2$ [60], which can probe our DM scenario.

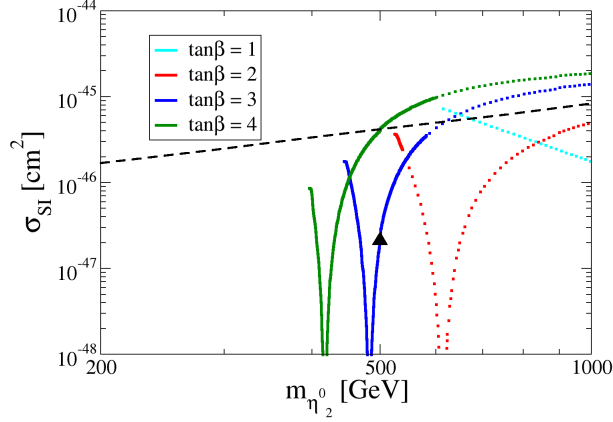


FIG. 10. DM mass versus spin-independent cross section. The cyan, red, blue and green lines show the results for $\tan\beta = 1, 2, 3$ and 4 , respectively, for $m_{h_2} = 200$ GeV, $m_{H^\pm} = m_{A_1} = 250$ GeV, and $m_A = m_{\eta^\pm} = m_{\eta^0} + 20$ GeV. The dotted lines are excluded by the unitarity and the bounded-from-below conditions on the scalar potential [48]. The region above the black dashed line is excluded by XENON1T [60].

VI. CONCLUSION

We have studied the neutrino mass matrix that is composed of the four flavor structures in Eq. (3) based on the A_4 flavor symmetry, focusing on the hierarchical flavor structures. As a model with a large hierarchical structure, we have proposed a hybrid seesaw model based on the A_4 flavor symmetry. In the model, the neutrino masses are generated by the tree-level and the one-loop seesaw mechanisms. These mechanisms induce different flavor structures and the large hierarchy with $|b|/|d| > \pi^2$ via the A_4 triplet fields of the right-handed neutrinos at the intermediate scale and of the scalar doublet at the electroweak scale. The non-zero θ_{13} is generated by the one-loop seesaw mechanism. The model predicts a large effective neutrino mass $m_{ee} \sim 0.03$ eV, which can be tested by future $0\nu\beta\beta$ experiments, with a Majorana phase $\alpha_3 \sim 0$. Furthermore, the A_4 flavor symmetry is broken down to the Z_2 symmetry in our model and the Z_2 -odd scalar field η_2^0 becomes the DM. The constraints arising from the DM relic density set its mass in the range of $400 \text{ GeV} \lesssim m_{\eta_2^0} \lesssim 600 \text{ GeV}$. Future direct detection experiments such as XENONnT will be able to access our DM scenario.

We have also performed a model-independent analysis of the neutrino mass matrix in Eq. (3), particularly for the cases with some hierarchical flavor structures. It has been found that the hierarchical cases with $|b|/|a| > 1$, $|b|/|c| > 1$, and $|d|/|a| > 1$ reduce the allowed parameter space and show characteristic predictions for the Majorana phases. On the other hand, the hierarchical

case with $|b|/|d| > 1$ does not show specific predictions. However, a larger hierarchy with $|b|/|d| > \pi^2$, which can be realized in our hybrid seesaw model, can reduce the predicted parameter region, which will be testable by future $0\nu\beta\beta$ experiments.

ACKNOWLEDGMENTS

The work of M. A. is supported in part by the Japan Society for the Promotion of Sciences Grant-in-Aid for Scientific Research (Grant No. 17K05412 and No. 20H00160).

-
- [1] P. Minkowski. $\mu \rightarrow e\gamma$ at a Rate of One Out of 10^9 Muon Decays? *Phys. Lett. B*, 67:421–428, 1977.
 - [2] R. N. Mohapatra and G. Senjanovic. Neutrino Mass and Spontaneous Parity Nonconservation. *Phys. Rev. Lett.*, 44:912, 1980.
 - [3] M. Gell-Mann, P. Ramond, and R. Slansky. Complex Spinors and Unified Theories. *Conf. Proc. C*, 790927:315–321, 1979.
 - [4] J. Schechter and J. Valle. Neutrino Masses in $SU(2) \times U(1)$ Theories. *Phys. Rev. D*, 22:2227, 1980.
 - [5] T. Yanagida. Horizontal Symmetry and Masses of Neutrinos. *Prog. Theor. Phys.*, 64:1103, 1980.
 - [6] A. Zee. A Theory of Lepton Number Violation, Neutrino Majorana Mass, and Oscillation. *Phys. Lett. B*, 93:389, 1980. [Erratum: *Phys.Lett.B* 95, 461 (1980)].
 - [7] A. Zee. Quantum Numbers of Majorana Neutrino Masses. *Nucl. Phys. B*, 264:99–110, 1986.
 - [8] K. Babu. Model of ‘Calculable’ Majorana Neutrino Masses. *Phys. Lett. B*, 203:132–136, 1988.
 - [9] L. M. Krauss, S. Nasri, and M. Trodden. A Model for neutrino masses and dark matter. *Phys. Rev. D*, 67:085002, 2003.
 - [10] E. Ma. Verifiable radiative seesaw mechanism of neutrino mass and dark matter. *Phys. Rev. D*, 73:077301, 2006.
 - [11] M. Aoki, S. Kanemura, and O. Seto. Neutrino mass, Dark Matter and Baryon Asymmetry via TeV-Scale Physics without Fine-Tuning. *Phys. Rev. Lett.*, 102:051805, 2009.
 - [12] M. Gustafsson, J. M. No, and M. A. Rivera. Predictive Model for Radiatively Induced Neutrino Masses and Mixings with Dark Matter. *Phys. Rev. Lett.*, 110(21):211802, 2013. [Erratum: *Phys.Rev.Lett.* 112, 259902 (2014)].
 - [13] Y. Cai, T. Han, T. Li, and R. Ruiz. Lepton Number Violation: Seesaw Models and Their Collider Tests. *Front. in Phys.*, 6:40, 2018.
 - [14] K. Abe et al. Atmospheric neutrino oscillation analysis with external constraints in Super-Kamiokande I-IV. *Phys. Rev. D*, 97(7):072001, 2018.
 - [15] G. Bak et al. Measurement of Reactor Antineutrino Oscillation Amplitude and Frequency at RENO. *Phys. Rev. Lett.*, 121(20):201801, 2018.
 - [16] M. Acero et al. First Measurement of Neutrino Oscillation Parameters using Neutrinos and Antineutrinos by NOvA. *Phys. Rev. Lett.*, 123(15):151803, 2019.
 - [17] H. d Kerret et al. Double Chooz θ_{13} measurement via total neutron capture detection. *Nature Phys.*, 16(5):558–564, 2020.

- [18] K. Abe et al. T2K measurements of muon neutrino and antineutrino disappearance using 3.13×10^{21} protons on target. 8 2020.
- [19] I. Esteban, M. Gonzalez-Garcia, M. Maltoni, T. Schwetz, and A. Zhou. The fate of hints: updated global analysis of three-flavor neutrino oscillations. *JHEP*, 09:178, 2020.
- [20] G. Altarelli and F. Feruglio. Discrete Flavor Symmetries and Models of Neutrino Mixing. *Rev. Mod. Phys.*, 82:2701–2729, 2010.
- [21] H. Ishimori, T. Kobayashi, H. Ohki, Y. Shimizu, H. Okada, and M. Tanimoto. Non-Abelian Discrete Symmetries in Particle Physics. *Prog. Theor. Phys. Suppl.*, 183:1–163, 2010.
- [22] S. F. King and C. Luhn. Neutrino Mass and Mixing with Discrete Symmetry. *Rept. Prog. Phys.*, 76:056201, 2013.
- [23] S. F. King, A. Merle, S. Morisi, Y. Shimizu, and M. Tanimoto. Neutrino Mass and Mixing: from Theory to Experiment. *New J. Phys.*, 16:045018, 2014.
- [24] S. King. Unified Models of Neutrinos, Flavour and CP Violation. *Prog. Part. Nucl. Phys.*, 94:217–256, 2017.
- [25] M. J. Pérez, M. H. Rahat, P. Ramond, A. J. Stuart, and B. Xu. Stitching an asymmetric texture with $T_{13} \times Z_5$ family symmetry. *Phys. Rev. D*, 100(7):075008, 2019.
- [26] F. Feruglio. *Are neutrino masses modular forms?*, pages 227–266. 2019.
- [27] G. Altarelli and F. Feruglio. Tri-bimaximal neutrino mixing, $A(4)$ and the modular symmetry. *Nucl. Phys. B*, 741:215–235, 2006.
- [28] P. Harrison, D. Perkins, and W. Scott. Tri-bimaximal mixing and the neutrino oscillation data. *Phys. Lett. B*, 530:167, 2002.
- [29] Y. Shimizu, M. Tanimoto, and A. Watanabe. Breaking Tri-bimaximal Mixing and Large θ_{13} . *Prog. Theor. Phys.*, 126:81–90, 2011.
- [30] D. Aristizabal Sierra and I. d Medeiros Varzielas. Reactor mixing angle from hybrid neutrino masses. *JHEP*, 07:042, 2014.
- [31] B. Karmakar and A. Sil. An A_4 realization of inverse seesaw: neutrino masses, θ_{13} and leptonic non-unitarity. *Phys. Rev. D*, 96(1):015007, 2017.
- [32] P. Novichkov, S. Petcov, and M. Tanimoto. Trimaximal Neutrino Mixing from Modular A_4 Invariance with Residual Symmetries. *Phys. Lett. B*, 793:247–258, 2019.
- [33] T. Kobayashi, Y. Shimizu, K. Takagi, M. Tanimoto, and T. H. Tatsuishi. A_4 lepton flavor model and modulus stabilization from S_4 modular symmetry. *Phys. Rev. D*, 100(11):115045, 2019. [Erratum: Phys.Rev.D 101, 039904 (2020)].
- [34] H. Okada and M. Tanimoto. Quark and lepton flavors with common modulus τ in A_4 modular symmetry. 5 2020.
- [35] S.-L. Chen, M. Frigerio, and E. Ma. Hybrid seesaw neutrino masses with $A(4)$ family symmetry. *Nucl. Phys. B*, 724:423–431, 2005.
- [36] D. Borah, S. Patra, and P. Pritimita. Sub-dominant type-II seesaw as an origin of non-zero θ_{13} in $SO(10)$ model with TeV scale Z' gauge boson. *Nucl. Phys. B*, 881:444–466, 2014.
- [37] D. Borah. Type II Seesaw Origin of Nonzero θ_{13}, δ_{CP} and Leptogenesis. *Int. J. Mod. Phys. A*, 29:1450108, 2014.
- [38] Y. Hamada, T. Kobayashi, A. Ogasahara, Y. Omura, F. Takayama, and D. Yasuhara. Revisiting discrete dark matter model: $\theta_{13} \neq 0$ and ν_R dark matter. *JHEP*, 10:183, 2014.
- [39] A. Mukherjee and M. K. Das. Neutrino phenomenology and scalar Dark Matter with A_4 flavor symmetry

- in Inverse and type II seesaw. *Nucl. Phys. B*, 913:643–663, 2016.
- [40] S. Pramanick and A. Raychaudhuri. A_4 -based seesaw model for realistic neutrino masses and mixing. *Phys. Rev. D*, 93(3):033007, 2016.
 - [41] E. T. Franco. Type I+III seesaw mechanism and CP violation for leptogenesis. *Phys. Rev. D*, 92(11):113010, 2015.
 - [42] S. Pramanick. Ameliorating the popular lepton mixings with A_4 symmetry: A seesaw model for realistic neutrino masses and mixing. *Phys. Rev. D*, 98(7):075016, 2018.
 - [43] D. Borah and B. Karmakar. A_4 flavour model for Dirac neutrinos: Type I and inverse seesaw. *Phys. Lett. B*, 780:461–470, 2018.
 - [44] R. A. Laamara, M. Loualidi, M. Miskaoui, and E. Saidi. Hybrid seesaw neutrino model in SUSY $SU(5) \times A_4$. *Phys. Rev. D*, 98(1):015004, 2018.
 - [45] S. Mishra. Majorana dark matter and neutrino mass with S_3 symmetry. *Eur. Phys. J. Plus*, 135(6):485, 2020.
 - [46] X. Wang. Lepton flavor mixing and CP violation in the minimal type-(I+II) seesaw model with a modular A_4 symmetry. *Nucl. Phys. B*, 957:115105, 2020.
 - [47] L. M. De La Vega, R. Ferro-Hernandez, and E. Peinado. Simple A_4 models for dark matter stability with texture zeros. *Phys. Rev. D*, 99(5):055044, 2019.
 - [48] M. Boucenna, M. Hirsch, S. Morisi, E. Peinado, M. Taoso, and J. Valle. Phenomenology of Dark Matter from A_4 Flavor Symmetry. *JHEP*, 05:037, 2011.
 - [49] N. Aghanim et al. Planck 2018 results. VI. Cosmological parameters. *Astron. Astrophys.*, 641:A6, 2020.
 - [50] J. Albert et al. Sensitivity and Discovery Potential of nEXO to Neutrinoless Double Beta Decay. *Phys. Rev. C*, 97(6):065503, 2018.
 - [51] M. Hirsch, S. Morisi, E. Peinado, and J. Valle. Discrete dark matter. *Phys. Rev. D*, 82:116003, 2010.
 - [52] E. Peinado. Dark Matter Stability from Non-Abelian Discrete Flavor Symmetries. *J. Phys. Conf. Ser.*, 375:012043, 2012.
 - [53] S. Bhattacharya, B. Karmakar, N. Sahu, and A. Sil. Flavor origin of dark matter and its relation with leptonic nonzero θ_{13} and Dirac CP phase δ . *JHEP*, 05:068, 2017.
 - [54] J. Lamprea and E. Peinado. Seesaw scale discrete dark matter and two-zero texture Majorana neutrino mass matrices. *Phys. Rev. D*, 94(5):055007, 2016.
 - [55] N. Gautam and M. K. Das. Phenomenology of keV scale sterile neutrino dark matter with S_4 flavor symmetry. *JHEP*, 01:098, 2020.
 - [56] L. Lopez Honorez, E. Nezri, J. F. Oliver, and M. H. Tytgat. The Inert Doublet Model: An Archetype for Dark Matter. *JCAP*, 02:028, 2007.
 - [57] R. Barbieri, L. J. Hall, and V. S. Rychkov. Improved naturalness with a heavy Higgs: An Alternative road to LHC physics. *Phys. Rev. D*, 74:015007, 2006.
 - [58] A. Goudelis, B. Herrmann, and O. Stål. Dark matter in the Inert Doublet Model after the discovery of a Higgs-like boson at the LHC. *JHEP*, 09:106, 2013.
 - [59] J. R. Ellis, A. Ferstl, and K. A. Olive. Reevaluation of the elastic scattering of supersymmetric dark matter. *Phys. Lett. B*, 481:304–314, 2000.
 - [60] E. Aprile et al. First Dark Matter Search Results from the XENON1T Experiment. *Phys. Rev. Lett.*, 119(18):181301, 2017.